Journal of Materials Chemistry

www.rsc.org/materials

Volume 19 | Number 9 | 7 March 2009 | Pages 1193–1340

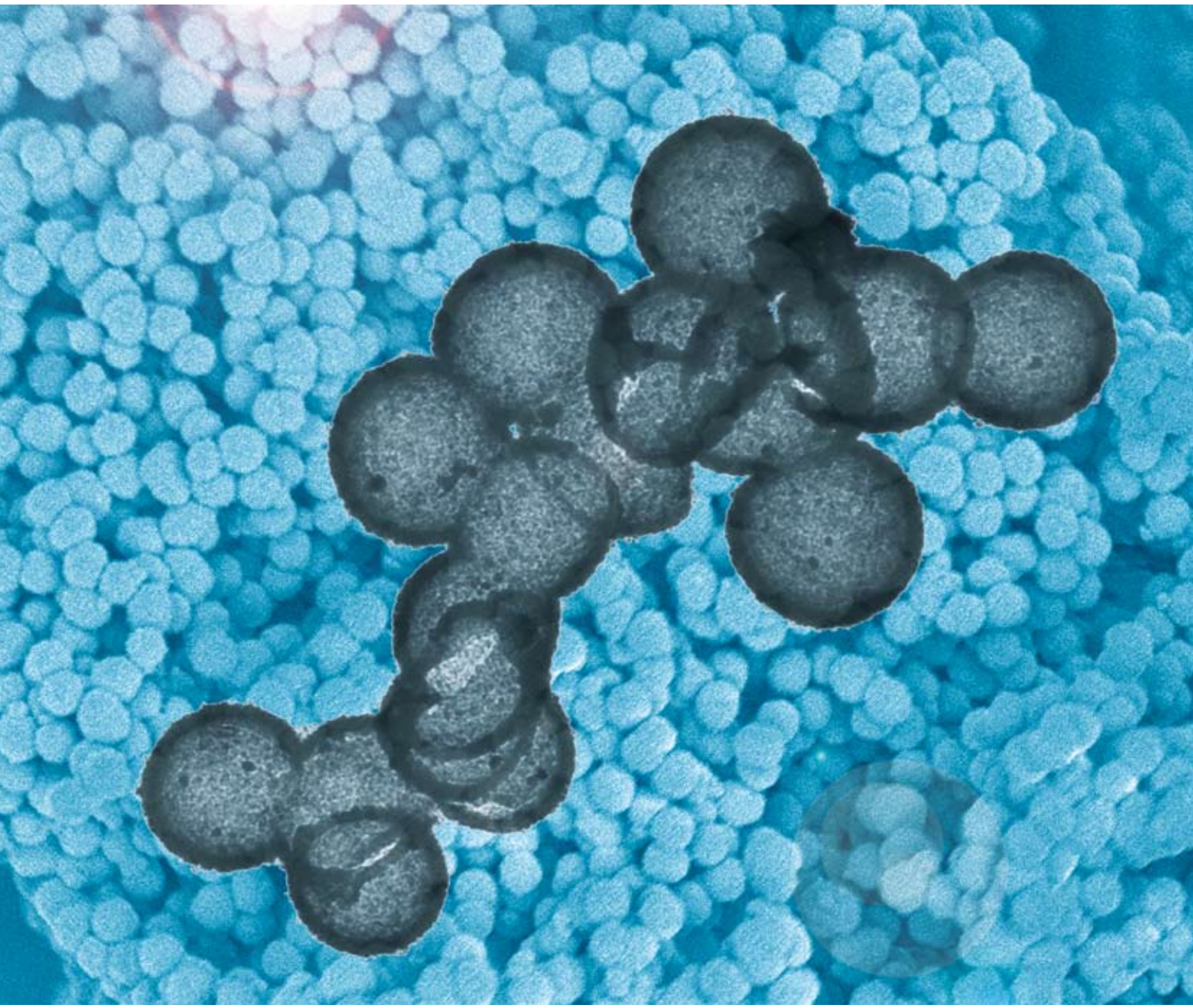

ISSN 0959-9428

RSC Publishing

0959-9428(2009)19:7;1-9

Magnetic Ni/SiO_2 composite microcapsules prepared by one-pot synthesis†

Chifeng Tu,[a] Jingjie Du,[b] Li Yao,[a] Chunhui Yang,[a] Maofa Ge,[a] Chuanlai Xu*[b] and Mingyuan Gao*[a]

Received 23rd September 2008, Accepted 5th November 2008
First published as an Advance Article on the web 12th December 2008
DOI: 10.1039/b816568h

The Ni/SiO_2 composite microcapsules were prepared by a one-pot synthesis *via* thermally decomposing $Ni(acac)_2 \cdot 2H_2O$ in 2-pyrrolidone in the presence of tetraethyloxysilane and 3-aminopropyltrimethoxysilane (APS). Transmission electron microscopy and powder X-ray diffraction were used to characterize the general morphology of the resultant capsules as well as the crystalline phases of the Ni nanocrystals incorporated. Ultraviolet photoelectron spectroscopy and ultraviolet photoionization mass spectroscopy were adopted to analyze the gaseous species released during the reaction to elucidate the mechanism behind the formation of the Ni/SiO_2 composite microcapsules. Preliminary experiments were designed to show the catalytic ability of the resultant capsules which were collectable by applying an external magnetic field.

Introduction

Recently, hollow capsules with diameters in a size range of nanometer to micrometer have attracted more and more attention due to their potential applications in various fields such as drug delivery, catalysis, smart materials with self-healing functions *etc*.[1] Even though different synthetic routes have been developed for fabricating stable hollow capsules of different materials,[2] removable templates remain non-substitutive in all synthetic routes. In general, the removable templates can further be classified into two groups, *i.e.*, rigid templates and soft templates. The biggest advantage of using rigid templates is the availability of highly uniform capsules. Polymeric latexes and colloidal SiO_2 particles are representative of the rigid templates.[3] By ionic layer-by-layer coating or controllable surface reactions, both soft and rigid capsules with uniform sizes have been achieved.[4] Very recently, the rigid templates have been further extended to nanometer sized colloidal particles to achieve nanocapsules upon various displacement reactions.[5] Nevertheless, removal of the templates is generally required with respect to the rigid-template approaches. On the contrary, the soft template routes, in most cases, require no specific procedures for removing the templates as they are typically formed by microemulsion droplets,[6] liquid droplets,[7] surfactant vesicles,[8] acoustic cavitation[9] and polymer micelles.[10] However, the uniformity of the resultant capsules is consequently sacrificed due to the size fluctuation of the soft templates.

Inorganic nanocrystals have been demonstrated to possess special properties which greatly differ from those of their corresponding bulks. Therefore, remarkable properties are expected from capsules composed of various types of nanomaterials of transition metals, noble metals and semiconductors.[2,3c] The preparation of capsules incorporated with Ni nanoparticles may lead to a new type of functional material due to the fact that Ni is characterized by its fascinating magnetism and excellent catalytic properties.[11] In fact, there exist two types of crystalline phase with respect to metal Ni, *i.e.*, the face-centered cubic phase (fcc phase) and the hexagonal close-packed phase (hcp phase). The former is stable in nature and susceptible to magnetism, while the latter is documented to be metastable and antiferromagnetic.[12] Control over the crystalline phase of Ni nanoparticles in the resultant capsules therefore becomes another important issue with respect to the preparation of capsules incorporated with Ni nanoparticles.

Herein, we report a facile synthetic route for Ni/SiO_2 composite capsules. As previously demonstrated, strong polar 2-pyrrolidone can serve as a coordinating solvent for preparing water-soluble magnetite nanocrystals *via* a "one-pot" reaction in addition to offering a high temperature environment.[13] By a similar strategy, the SiO_2 capsules incorporated by Ni nanoparticles were prepared in 2-pyrrolidone by thermally decomposing $Ni(acac)_2 \cdot 2H_2O$ [nickel(II)biacetylacetonate] in the presence of TEOS (tetraethyloxysilane) and APS (3-aminopropyltrimethoxysilane). The formation mechanism leading to the unexpected hollow SiO_2 capsules incorporated with Ni nanoparticles was investigated. Furthermore, the control over the crystalline structure of the Ni nanoparticles was also studied.

Experimental

Chemicals

Tetraethyloxysilane (TEOS, 98%) and 3-aminopropyltrimethoxysilane (APS, 98%) were purchased from Fluka and used without further purification. $Ni(acac)_2 \cdot 2H_2O$ was received from Aldrich. 2-Pyrrolidone was purified under vacuum distillation before use. Methylene blue trihydrate (MBt) and sodium borohydride ($NaBH_4$) were supplied by Sinopharm. Chemical Co., Ltd (China) and used as received.

[a]*Institute of Chemistry, Chinese Academy of Sciences, Bei Yi Jie 2, Zhong Guan Cun, Beijing, 100190, China. E-mail: gaomy@iccas.ac.cn; Fax: +010 82613214; Tel: +010 82613214*
[b]*School of Food Science and Technology, Jiangnan University, Lihu Road 1800, Wuxi, Jiangsu Province, 214122, China. E-mail: xcl@jiangnan.edu.cn*

† Electronic supplementary information (ESI) available: (1) thermal decomposition behavior of $Ni(acac)_2 \cdot 2H_2O$, (2) control experiment of sample 1, (3) pore-size analysis on sample 1, (4) SEM investigations on samples 4–6, (5) crystalline phase analysis on sample 4–6. See DOI: 10.1039/b816568h

Preparation of Ni/SiO_2 composite microcapsules

In a typical preparation, 0.4 g of $Ni(acac)_2 \cdot 2H_2O$ (1.37 mmol) was introduced into a three-necked flask followed by 20 mL 2-pyrrolidone. With the aid of magnetic stirring, the nickel(II) precursor was dissolved after the reaction temperature was slowly elevated to 60 °C, resulting in a light-green transparent solution. Then, 243 μL of APS (1.37 mmol) and 155 μL of TEOS (0.68 mmol) were injected into the reaction solution. With the increase of reaction temperature, the viscosity of the reaction system apparently increased from around 70 °C followed by a color variation of the reaction mixture from transparent green to turbid blue at ~80 °C. Meanwhile unknown gaseous species were released from the reaction system, leading to tiny gas bubbles evenly distributed throughout the reaction mixture. The color of the reaction mixture evolved from turbid blue to black *via* light yellow upon further increase of the reaction temperature. The final samples were typically obtained by heating the reaction solution for 5 hours at designed temperatures, *i.e.*, 200 °C for sample 1, 220 °C for sample 2, and 245 °C for sample 3, respectively. Throughout the preparation, the reaction solution was continuously purged with nitrogen gas to avoid any unwanted oxidation by oxygen. After the preparation, the reaction mixture was cooled down to room temperature, then a 4-fold volume of ether was added into the resultant solution to precipitate the capsules which were subsequently washed with ethanol 3 times and finally dried for characterization. To further investigate the effect of concentration of the different reagents involved, the following experiments were carried out for preparing samples 4–6; details are given in Table 1. The reaction temperature was set to 200 °C and the reaction time was fixed at 5 h.

Catalytic properties of the Ni/SiO_2 composite microcapsules

MBt was chosen as a model compound to test the catalytic properties of the resultant capsules. The experiments were carried out as follows. Powder of the composite microcapsules (18 mg, sample 5) was dissolved in 5 mL ethanol. In parallel, 35 mL aqueous solution containing 5 mg (13 μmol) MBt was prepared. Then, these two solutions were mixed under stirring. The color variation of the reaction mixture was monitored using an ultra-violet–visible absorption spectrometer after 10 mL aqueous solution of $NaBH_4$ (2.2 mM) was rapidly introduced.

Characterization

Transmission electron microscopy (TEM) images and selected-area electron diffraction (SAED) patterns were recorded with a JEM-100CX II microscope operating at an accelerating voltage of 100 kV. XRD patterns were obtained with a Rigaku D/Max-2500 diffractometer equipped with a rotating anode and a Cu kα1 radiation source ($\lambda = 1.54056$ Å). The magnetic hysteresis loops of the resultant capsules were recorded with a vibrating sample magnetometer (VSM, JDM-13). UV-Vis absorption spectra were recorded with a Cary 50 spectrophotometer. The nickel content in the resultant capsules was determined using an inductive coupled plasma (ICP) emission spectrometer (Thermo Electron Corp). The small molecular weight species released during the preparation were analyzed with a home-made instrument combining both ultraviolet photoelectron spectroscopy and ultraviolet photoionization mass spectroscopy (PES-PIMS). Argon and methyl iodide were used as internal standards for the measurements.[14]

Results and discussion

Fig. 1 shows representative TEM images of samples 1–3 prepared at 200, 220 and 245 °C, respectively. All these samples are mainly

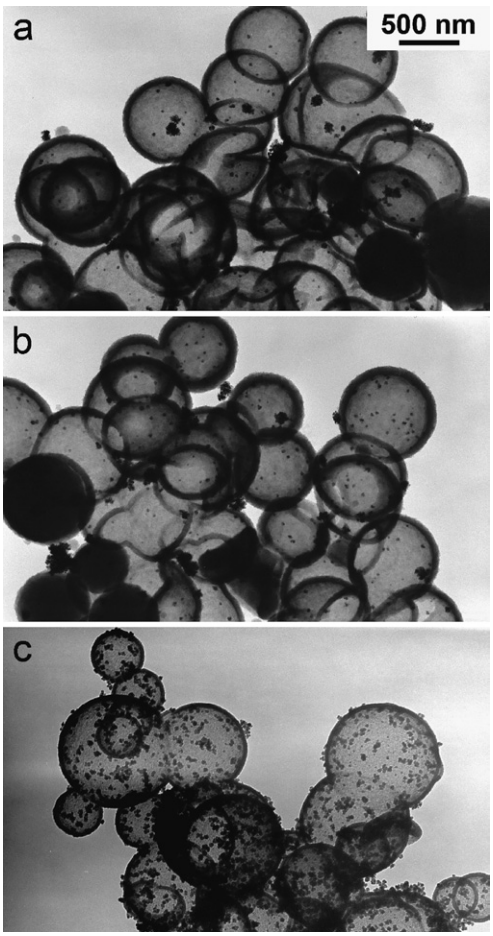

Fig. 1 Representative TEM images of the composite capsules in sample 1 (a), sample 2 (b), and sample 3 (c), respectively.

Table 1 Detailed methods for samples 4–6

	Sample 4	Sample 5	Sample 6
$Ni(acac)_2$ $2H_2O$	0.4 g (1.37 mmol)	0.2 g (0.68 mmol)	0.1 g (0.34 mmol)
Silane precursors	121 μL (0.68 mmol) APS 77μL (0.34 mmol) TEOS	61 μL (0.34 mmol) APS 39 μL (0.17 mmol) TEOS	30 μL (0.17 mmol) APS 19 μL (0.085 mmol) TEOS

composed of spherical hollow capsules of 200–800 nm with some of them being inter-connected forming larger hollow structures. The thickness of the capsule shell is generally in the range of 40–80 nm. In addition, there are small particles shown as black dots incorporated into the capsule shells (some of them apparently appearing on the surface of the capsules, especially with respect to sample 3). In general, the dots increase in size and quantity against the reaction temperature.

The crystal structure of the nanoparticles showing in the microcapsules in Fig. 1 was further analyzed by X-ray diffraction. The XRD patterns of samples 1–3 are shown in Fig. 2a–c, respectively. It is quite obvious that sample 1 consists of cubic phase Ni nanoparticles according to standard data (JCPDS No. 04-0850) provided, and sample 3 consists of pure hexagonal Ni nanocrystals (JCPDS No. 45-1027), while the sample prepared at 220 °C (sample 2) consists of particles with a mixed crystalline structure of both cubic and hexagonal phases. Careful observation reveals that the diffraction peaks are sharpened by the increased temperature. By taking the phase assignments into consideration, the average size of Ni nanocrystals was estimated to increase from 8.9 nm for sample 1 to 15.7 nm for sample 3, using the Scherrer equation and XRD results. This size increment is generally in a very good agreement with the TEM results shown in Fig. 1, suggesting that the black dots incorporated in the capsule shells are Ni nanocrystals, while the broad diffraction peak between 15° and 33° implies that the microcapsules are mainly formed by amorphous silica according to previous investigations.[15]

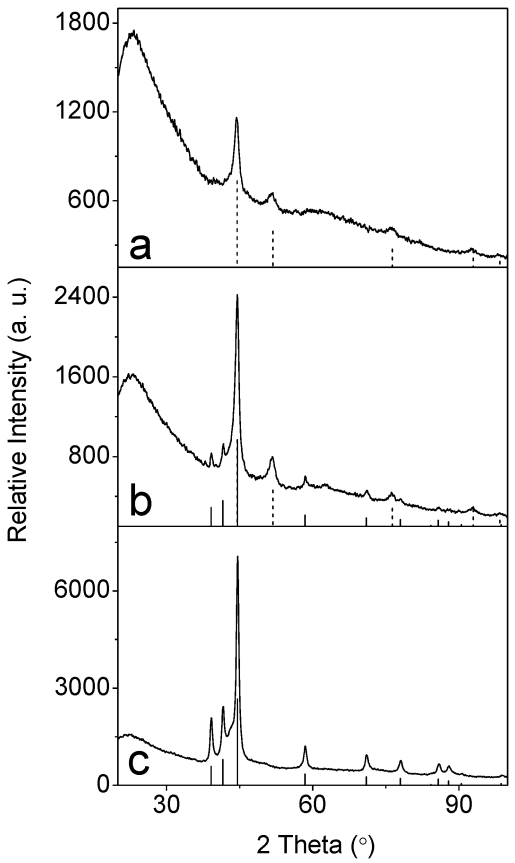

Fig. 2 XRD patterns of sample 1 (a), sample 2 (b), and sample 3 (c). The line patterns shown at the bottom of each frame are standard data from JCPDS cards with dashed and solid lines corresponding to cubic and hexagonal Ni, respectively.

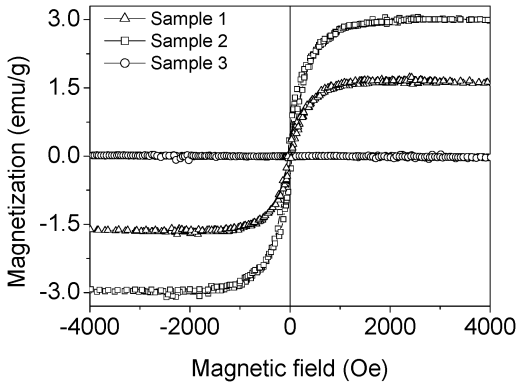

Fig. 3 Room temperature hysteresis curves recorded from samples 1–3.

As the magnetic property of nickel is strongly phase-dependent, samples 1–3 were investigated by VSM. The hysteresis loops of samples 1–3 shown in Fig. 3 suggest that samples 1 and 2 are superparamagnetic with a saturation magnetization of 1.6 and 3.0 emu g^{-1}, respectively, while sample 3 is anti-ferromagnetic. In other words, the saturation magnetization of the capsules presents a non-monotonic behavior against the reaction temperature, and maintains the same tendency after excluding the difference of the Ni content in samples 1–2 determined by ICP measurements. Details are shown in Table 2.

It is known that cubic phase Ni is ferromagnetic with a saturation magnetization of ~55 emu g^{-1}, while hexagonal phase Ni is anti-ferromagnetic at room temperature. Therefore, that sample 2 presents higher saturation magnetization than sample 1 can be attributed partly to the increased particle size and partly to the enhanced degree of crystallinity of the incorporated Ni nanoparticles, even though hcp phase Ni starts to be formed at 220 °C (sample 2).

To the best of our knowledge, the current synthetic approach sets the first example for preparing silica microcapsules incorporated with inorganic nanocrystals *via* a "one-pot" synthesis. As mentioned in the introduction templates are essential for capsule synthesis. It is interesting to know what acted as a template in the current synthetic route, as the initial idea was to prepare solid silica particles incorporated with Ni nanocrystals rather than hollow capsules. Therefore, the following experiments were carried out to discover the nature and the formation of the template in the current synthesis.

The role of APS in the decomposition of $Ni(acac)_2 \cdot 2H_2O$ was firstly investigated by UV-Vis spectroscopy. It has previously been demonstrated that amine can catalyze the sol–gel process of silica.[16] Moreover, it can also coordinate with metal ions and

Table 2 Magnetic properties of samples 1–2

Sample	Phase	Ms/emu g^{-1}	Ni content (%)	Normalized Ms/emu g^{-1}
1	fcc	1.7	14.05	12.1
2	hcp + fcc	3	20.15	14.8

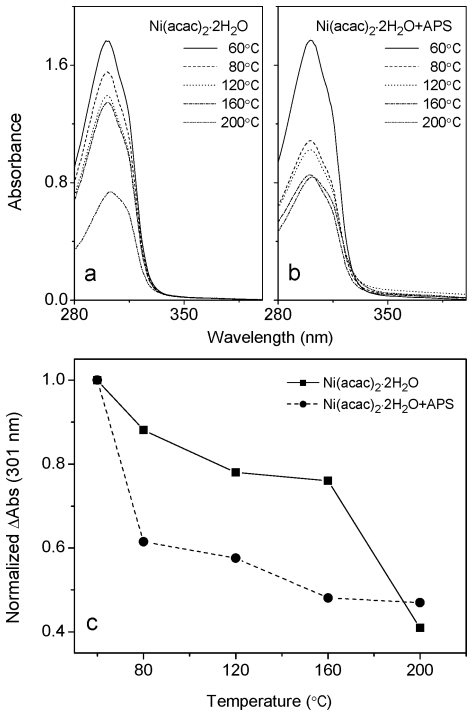

Fig. 4 Upper panel: UV-Vis absorption spectra recorded at different temperatures for monitoring the thermal decomposition of $Ni(acac)_2 \cdot 2H_2O$ in the absence (a) or presence (b) of APS. Lower panel: absorbance variations against reaction time at 301 nm.

anchor on the surface of the resultant metal or metal oxide nanoparticles.[11c] Therefore, it would be interesting to discover the role of the amine group from APS used in the current synthesis. Two sets of experiments were performed by pyrolyzing an identical amount of $Ni(acac)_2 \cdot 2H_2O$ in 2-pyrrolidone in the absence of APS (Fig. 4a) or in the presence of APS (Fig. 4b). According to the literature,[17] the absorption at around 301 nm shown in Fig. 4a,b can be attributed to a π–π^* transition of $Ni(acac)_2$. Therefore, the absorbance at 301 nm was recorded from both reaction systems and compared in Fig. 4c. It is quite obvious that APS greatly decreases the decomposition temperature, consequently a fast decay of the $Ni(acac)_2$ concentration appears below 80 °C rather than above 160 °C for a former system without APS. The results of TGA, shown in Figure S1†, demonstrate that $Ni(acac)_2$ starts to decompose at 183 °C in nitrogen, it can thus be concluded that APS greatly contributes to the early decomposition occurring between 60 °C and 80 °C, which is exactly the temperature range where the reaction system started to release gaseous species and changed in both color and viscosity as mentioned in the Experimental section.

Another control experiment was designed by replacing $Ni(acac)_2 \cdot 2H_2O$ with equal amounts of anhydrous $Fe(acac)_3$ and the equivalent amount of water to further elucidate the mechanism for the increased viscosity of the reaction system. However, under exactly the same preparative conditions for creating silica capsules incorporated with Ni nanocrystals, no silica capsules were obtained (Figure S2†) and throughout the reaction the viscosity of the reaction system remained nearly unchanged, which suggests that the aforementioned viscosity increase is caused by the formation of coordination polymer networks involving $Ni(acac)_2$ and APS, rather than hydrolysis of silane precursors due to the existence of the trace crystal water carried by $Ni(acac)_2$. Consequently, by taking advantage of the gaseous species generated during the reaction, tiny gas bubbles enwrapped by polymeric gel formed by $Ni(acac)_2$ and APS with TEOS might be responsible for the formation of the capsules.

PES-PIMS was then adopted to identify the gaseous species generated during the early stage of the preparation. In detail, all gaseous species released during the reaction were carried by a nitrogen flow passing through a U-shaped glass tube immersed in liquid nitrogen. After that, the U-shaped tube connected to a double-chamber UPS machine-II, was slowly warmed up and consequently gaseous species entrapped in the U-tube were vaporized successively according to their boiling points, and then detected by a HeI photoelectron spectrometer coupled with an ultra-violet photoionization mass spectrometer.[14] The photoelectron spectra and the photoionization mass spectra of the gaseous species released during the earlier stage (below 120 °C) are shown in Fig. 5a,b and 6a,b respectively, while those recorded from gaseous species released at higher temperature are presented in Fig. 5c and 6c, respectively.

The PES spectrum in Fig. 5a presents two peaks located at around 13.76 eV and 18.06 eV, respectively, which are the characteristic signals for carbon dioxide.[18] The spectrum of the following gases presented in Fig. 5b shows two groups of peaks which can be ascribed to methanol (10.95, 12.69 and 15.15 eV) and acetone (9.69, 12.62, 14.08, and 15.60 eV), respectively, while the gaseous species released higher than 120 °C can be identified as acetone (Fig. 5c) according to literature data.[18] All these

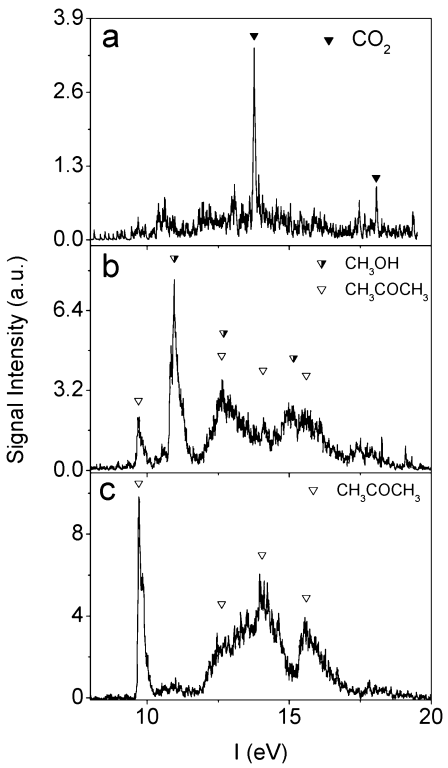

Fig. 5 HeI photoelectron spectra of the gaseous species collected below 120 °C (a, b) and above 120 °C (c), respectively, together with the corresponding identifications for gaseous species based on reference data.

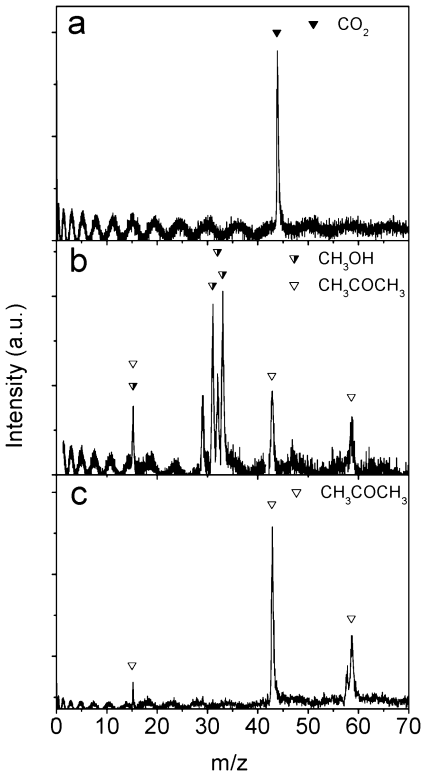

Fig. 6 HeI photoionization mass spectra of the gaseous species collected below 120 °C (a, b) and above 120 °C (c), respectively, together with the corresponding identifications for gaseous species based on reference data.

assignments are strongly supported by the ultra-violet photoionization mass spectroscopy results shown in Fig. 6. The signal at $m/z = 44$ shown in Fig. 6a confirms that the first gas to escape from the U-tube is carbon dioxide. The signals at $m/z = 15$, 31, 32, and 33 shown in Fig. 6b can be ascribed to fragment ions of methanol, while the signals at $m/z = 15$, 43, and 58 can be attributed to the fragment ions of acetone, according to the standard mass spectroscopy data of methanol and acetone.[19] Following these analyses, the spectrum shown in Fig. 6c demonstrates that the reaction system mainly generated acetone at temperatures higher than 120 °C apart from CO_2 (data not shown).

Based on the aforementioned results, the following conclusions can be reached: (1) APS can catalyze the decomposition of $Ni(acac)_2 \cdot 2H_2O$, leading to a greatly decreased decomposition temperature for $Ni(acac)_2 \cdot 2H_2O$; (2) APS can form a coordination polymer with $Ni(acac)_2 \cdot 2H_2O$, giving rise to the increased viscosity of the reaction system; (3) the early stage of the reaction generates gaseous species such as CO_2, methanol and acetone which work as a template for creating the hollow capsules shown in Fig. 1. In addition, the aforementioned results and analysis also enable the following mechanism to be reliable. APS coordinates with $Ni(acac)_2 \cdot 2H_2O$ *via* its amine group, which strongly weakens the stability of $Ni(acac)_2$. Catalyzed by the water of crystallization carried by $Ni(acac)_2$, the coordination polymer formed by APS and $Ni(acac)_2$ starts to hydrolyze with TEOS being involved *via* the sol–gel process, which leads to the increase in the viscosity of the reaction mixture. Further decomposition of Ni(II) precursor and the following condensation of APS and TEOS generates gaseous species forming small bubbles which are enwrapped by silica gel, eventually leading to the formation of the composite capsules. In other words, the coordination interaction between APS and nickel ions, the condensation of APS and TEOS, together with the decomposition of Ni(II) precursor have a collective effect on the formation of Ni/SiO_2 composite microcapsules. Further TEM observations and the N_2 sorption isotherm of Ni/SiO_2 microcapsules (shown in Figure S3†) indicate that the shell of composite microcapsules is nonporous, which further supports the mechanism that gaseous species act as the template for the formation of capsules. With respect to the formation of Ni nanocrystals, 2-pyrrolidone plays an important role as the slow thermal decomposition of 2-pyrrolidone generates reductant CO.[20]

According the mechanisms proposed above, the following experiments were carried out to further tune the morphology of the resultant capsules. In general, in comparison with the method used for sample 1, the molar ratio of silane to $Ni(acac)_2 \cdot 2H_2O$ was firstly halved to reduce the viscosity of the reaction mixture (sample 4). Following that, the concentration of all reagents was further halved (sample 5) and quartered (sample 6), as shown in Table 1, so that both the viscosity and the amount of gaseous species would be greatly reduced. TEM was used to characterize samples 4–6. The results shown in Fig. 7 demonstrate that the resultant particles become more and more uniform against the reduced concentration of reagents, which is accompanied by a structural transformation from hollow capsules to solid particles in addition to the decrease in particle size. Moreover, the resultant particles become more and more isolated. All this structure evolution can be understood as follows. As demonstrated above, the interaction between APS and $Ni(acac)_2$ plays a determined role in the gel formation during the reaction, therefore the reduced ratio of silane to $Ni(acac)_2$ will undoubtedly lead to a reduced size of the gel particles. When the initial concentration of $Ni(acac)_2$ was reduced from 0.068 M (sample 4) to 0.034 M (sample 5), the capsule shell became too thin to freely stand in the vacuum chamber for electron microscopy, consequently, all capsules in sample 5 are collapsed under TEM (Fig. 7b). In contrast, when the amount of $Ni(acac)_2$ enwrapped in the gel particles becomes too limited (sample 6), the silica/Ni nanocrystal composite particles exhibit solid instead of hollow structures as shown in Fig. 7c. Detailed SEM investigations on samples 4–6 are shown Figure S4 in the ESI†.

The phase structure of samples 4–6 was further characterized by XRD. The results shown in Figure S5† reveal that fcc is the dominant phase for Ni nanocrystals in all three samples except that hcp impurity is also presented in sample 4. In comparison with sample 1, sample 4 was prepared by halving the amount of APS. Therefore, the growth rate of Ni particles in the reaction system producing sample 4 should be faster than that for sample 1, as well as those for samples 5 and 6, as in the latter two systems the concentration of all reagents was reduced. It was previously demonstrated that a higher growth rate is generally in favor of a metastable hcp phase,[12a] which interprets the existence of hcp impurity in sample 4. The hcp impurity results in a reduced *Ms* (sample 4) in comparison with those for samples 5 and 6. Details are shown in Table 3.

It was experimentally demonstrated that metal Ni nanoparticles possess high catalytic activities for hydrogenation

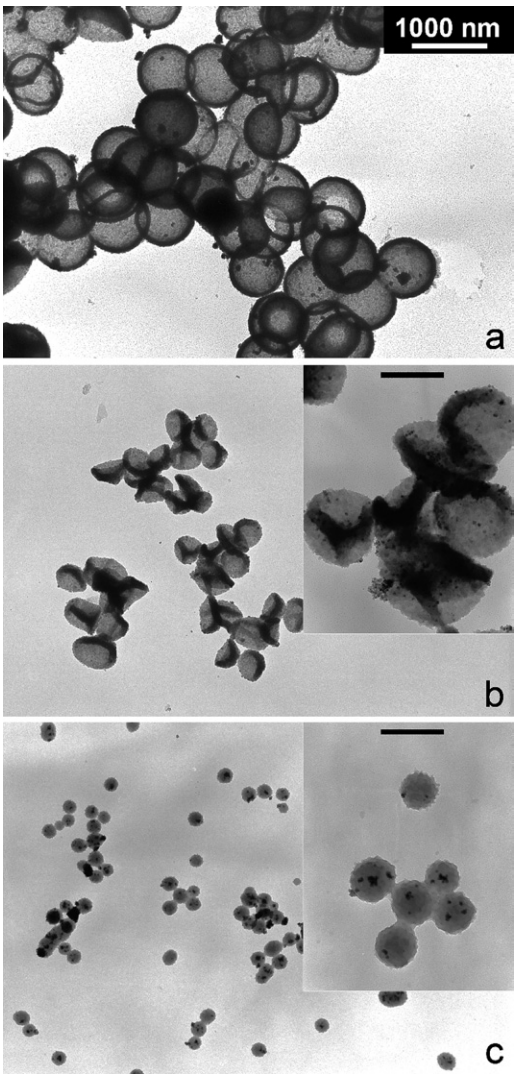

Fig. 7 Representative TEM images of sample 4 (a), sample 5 (b), and sample 6 (c). Insets are the enlarged images captured at a higher magnification; the scale bar corresponds to 200 nm.

Table 3 Magnetic properties of Samples 4–6

Sample	Phase	*Ms*/emu g^{-1}	Ni content (%)	Normalized *Ms*/emu g^{-1}
4	fcc + hcp	1.6	15.76	10.2
5	fcc	5.5	29.18	18.8
6	fcc	5.3	29.29	18.1

reactions.[21] Therefore, the catalytic properties of the composite capsules were investigated using MBt as a model compound. The preliminary results in Fig. 8 demonstrate that Ni/SiO_2 capsules (sample 5) can greatly accelerate the reduction reaction achieved by $NaBH_4$. As the capsule shell is mainly formed by silica as the matrix for Ni nanocrystals, the capsules can be homogenously dispersed in ethanol with the aid of mechanical stirring. However, they also present a quick response to magnetic fields as shown in Fig. 8.

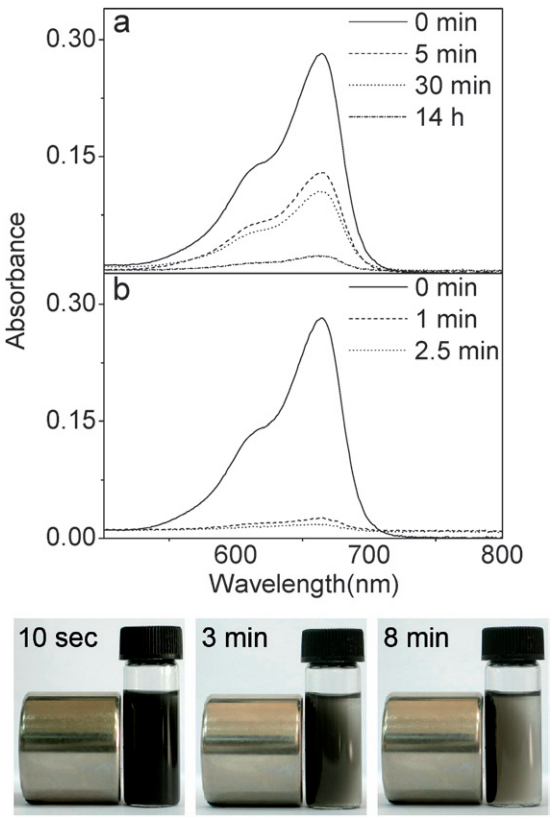

Fig. 8 Upper panel: UV-Vis absorption spectra of MBt recorded during the reduction reaction achieved by $NaBH_4$ in the absence (a) or presence of the Ni/SiO_2 capsules (sample 5), Lower panel: photographs of sample 5 dispersed in ethanol after being placed near to a permanent magnet for different periods of time.

Conclusions

In summary, a new type of Ni/SiO_2 composite microcapsules were prepared by pyrolyzing $Ni(acac)_2 \cdot 2H_2O$ in 2-pyrrolidone in the presence of APS and TEOS. Systematic investigations reveal that the interaction between APS and $Ni(acac)_2 \cdot 2H_2O$ can on the one hand reduce the temperature threshold for thermally decomposing $Ni(acac)_2 \cdot 2H_2O$, on the other hand initiate the sol–gel process with TEOS being involved. During the following reaction, gaseous species such as CO_2, methanol and acetone are released in the gel, eventually forming soft templates for the silica capsules. The Ni nanocrystals incorporated in the capsule shell are formed in different crystal phases depending on the molar ratio of silane to $Ni(acac)_2$ and the concentration of the reagents involved in addition to the reaction temperature. The composite capsules prepared under optimized conditions are rather monodispersed and well isolated. They present not only catalytic properties but also a strong response to external magnetic fields, leading to a recyclable composite catalyst.

Acknowledgements

This work was financially supported by NSFC projects (20673128, 20640430564).

References

1 (*a*) *Hollow and Solid Spheres and Microspheres: Science and technology associated with their fabrication and application*, ed. D. L. Wilcox, M. Berg, T. Bernat, D. Kellerman, J. K. Cochran, Materials Research Society Proceedings, Vol. 372, Pittsburgh, USA 1995, and references therein; (*b*) S. R. White, N. R. Sottos, P. H. Geubelle, J. S. Moore, M. R. Kessler, S. R. Sriram, E. N. Brown and S. Viswanathan, *Nature*, 2001, **409**, 794; (*c*) B. Comiskey, J. D. Albert, H. Yoshizawa and J. Jacobson, *Nature*, 1998, **394**, 253.

2 (*a*) C. Zimmermann, C. Feldmann, M. Wanner and D. Gerthsen, *Small*, 2007, **3**, 1347; (*b*) L. Guo, F. Liang, X. Wen, S. Yang, L. He, W. Zheng, C. Chen and Q. Zhong, *Adv. Funct. Mater.*, 2007, **17**, 425; (*c*) Q. Liu, H. Liu, M. Han, J. Zhu, Y. Liang, Z. Xu and Y. Song, *Adv. Mater.*, 2005, **17**, 1995.

3 (*a*) M. Chen, L. Wu, S. Zhou and B. You, *Adv. Mater.*, 2006, **18**, 801; (*b*) Y. Zhang, M. Jiang, J. Zhao, X. Ren, D. Chen and G. Zhang, *Adv. Funct. Mater.*, 2005, **15**, 695.

4 (*a*) F. Caruso, R. Caruso and H. Möhwald, *Science*, 1998, **282**, 1111; (*b*) D. Wang and F. Caruso, *Adv. Mater.*, 2003, **15**, 205.

5 (*a*) Y. Wang, L. Cai and Y. Xia, *Adv. Mater.*, 2005, **17**, 473; (*b*) K. Velikov and A. V. Blaaderen, *Langmuir*, 2001, **17**, 4779.

6 D. Walsh, B. Lebeau and S. Mann, *Adv. Mater.*, 1999, **11**, 324.

7 J. Huang, Y. Xie, B. Li, Y. Liu, Y. Qian and S. Zhang, *Adv. Mater.*, 2000, **12**, 808.

8 (*a*) C. A. McKelvey, E. W. Kaler, J. A. Zasadzinski, B. Coldren and H. T. Jung, *Langmuir*, 2000, **16**, 8285; (*b*) D. H. W. Hubert, M. Jung and A. L. German, *Adv. Mater.*, 2000, **12**, 1291.

9 R. K. Rana, Y. Mastai and A. Gedanken, *Adv. Mater.*, 2002, **14**, 1414.

10 (*a*) N. Botterhuis, Q. Sun, P. M. M. Magusin, R. V. Santen and N. J. M. Sommerdijk, *Chem. Eur. J.*, 2006, **12**, 1448; (*b*) T. Liu, Y. Xie and B. Chu, *Langmuir*, 2000, **16**, 9015.

11 (*a*) I. S. Lee, N. Lee, J. N. Park, B. H. Kim, Y. W. Yi, T. Kim, T. K. Kim, I. H. Lee, S. R. Paik and T. Hyeon, *J. Am. Chem. Soc.*, 2006, **128**, 10658; (*b*) J. Park, E. Kang, S. U. Son, H. M. Park, M. K. Lee, J. Kim, K. W. Kim, H. J. Noh, J. H. Park, C. J. Bae, J.-G. Park and T. Hyeon, *Adv. Mater.*, 2005, **17**, 429; (*c*) N. Cordente, M. Respaud, F. Senocq, M. J. Casanove, C. Amiens and B. Chaudret, *Nano Lett*, 2001, **1**, 565.

12 (*a*) M. Han, Q. Liu, J. He, Y. Song, Z. Xu and J. Zhu, *Adv. Mater.*, 2007, **19**, 1096; (*b*) Y. T. Jeon, J. Y. Moon and G. H. Lee, *J. Phys. Chem. B*, 2006, **110**, 1187.

13 Z. Li, H. Chen, H. B. Bao and M. Y. Gao, *Chem. Mater.*, 2004, **16**, 1391.

14 (*a*) L. Yao, X. Q. Zeng, M. F. Ge, W. G. Wang, Z. Sun, L. Du and D. X. Wang, *Eur. J. Inorg. Chem.*, 2006, **12**, 2469; (*b*) W. G. Wang, L. Yao, X. Q. Zeng, M. F. Ge, Z. Sun, D. X. Wang and Y. H. Ding, *J. Chem. Phys.*, 2006, **125**, 234303, (6 pages).

15 L. Y. Hao, C. L. Zhu, W. Q. Jiang, C. N. Chen, Y. Hu and Z. Y. Chen, *J. Mater. Chem.*, 2004, **14**, 2929.

16 N. Hüsing and U. Schubert, *Chem. Mater.*, 1999, **11**, 451.

17 R. H. Holm and F. A. Cotton, *J. Am. Chem. Soc.*, 1958, **80**, 5658.

18 K. Kimura, S. Katsumata, Y. Achiba, T. Yamazaki and S. Iwata, *Handbook of HeI Photoelectron Spectra of Fundamental Organic Molecules*, Japan Scientific Soc. Press, Tokyo, 1981.

19 NIST Chemistry WebBook, http://webbook.nist.gov/chemistry.

20 Z. Li, Q. Sun and M. Y. Gao, *Angew. Chem., Int. Ed.*, 2005, **44**, 123.

21 (*a*) P. Jin, Q. W. Chen, L. Q. Hao, R. F. Tian, L. X. Zhang and L. Wang, *J. Phys. Chem. B*, 2004, **108**, 6311; (*b*) M. Chen, J. Zhou, L. Xie, G. X. Gu and L. M. Wu, *J. Phys. Chem. C*, 2007, **111**, 11829.